JOURNAL OF SPACECRAFT AND ROCKETS
Vol. 44, No. 6, November–December 2007

Comparison of TIMED Satellite Drag with Solar EUV Experiment (SEE) Measurements

Donald L. Woodraska,* Thomas N. Woods,† and Francis G. Eparvier‡
University of Colorado, Boulder, Colorado 80303

DOI: 10.2514/1.28639

The Solar EUV Experiment (SEE) aboard the Thermosphere–Ionosphere–Mesosphere Energetics and Dynamics (TIMED) spacecraft measures the solar irradiance from 0.1–193 nm and has been operating from January 2002 to the present. The orientation of TIMED provides a stable, nearly constant, view factor to the ram direction. Together, the TIMED orientation and SEE measurements provide a unique opportunity to determine the influence of the solar radiation on satellite drag. This high-altitude upper-atmospheric satellite-drag study includes the determination of precision orbital changes of the TIMED spacecraft using the onboard global positioning system, validation of the drag estimate, identifying key wavelength ranges in the solar spectrum that affect the orbit changes, and creation of a solar irradiance index from those wavelengths that is representative of the atmospheric drag experienced by TIMED.

Nomenclature

a	=	semimajor axis
D	=	negative time rate of change of the semimajor axis
E	=	solar irradiance
n	=	mean motion
S_A	=	solar panel rotation angle about the panel centerline
T	=	nodal period
$\langle T \rangle_{15}$	=	15-orbit mean nodal period
t	=	time

I. Introduction

THIS paper presents a comparison of solar irradiance measurements and the observed orbit changes in NASA's Thermosphere–Ionosphere–Mesosphere Energetics and Dynamics (TIMED) spacecraft. Solar photons with wavelengths greater than 10 nm and shorter than 120 nm, referred to as extreme ultraviolet (EUV), are absorbed by Earth's atmosphere at altitudes above 90 km (the thermosphere). Photons with wavelengths from 120 to 200 nm, referred to as far ultraviolet (FUV), can be absorbed as low as 50 km (mesosphere) and higher into the thermosphere. Solar EUV creates the ionosphere and contributes to the heating of the thermosphere through the excess energy that remains after the processes of excitation and ionization. Photoelectrons are produced during ionization that further interact with neutrals causing excitation, dissociation, and additional ionization. FUV photons lead to photodissociation of molecules, photoionization of molecules and atoms, and photoexcitation. All of these processes play important roles in heating the thermosphere and provide some insight into the complexity of atmospheric chemistry and dynamics [1]. During periods of high solar activity, the solar EUV has been observed to increase by a factor of 2 or more [2]. The atmospheric drag forces experienced by spacecraft increase in response to thermospheric heating. The direct forcing of the atmosphere by solar EUV and FUV provides motivation for determining the relationship with satellite drag. In this paper, we will quantify the relationship between calibrated solar irradiance measurements and the measured orbit changes on TIMED. For this study, we focus on a narrow altitude region from 610–630 km.

The Solar EUV Experiment (SEE) is an instrument [2] onboard TIMED that nominally measures solar radiation once per orbit with about 0.4-nm resolution from 27–193 nm and broadband shortward of 27 nm. SEE has nearly a 3% duty cycle for observing the sun. This paper presents a comparison of solar irradiance measured by SEE and the TIMED orbital changes. Prior satellite-drag studies have been limited to using only proxies [3]; however, we propose that this is no longer necessary because SEE has been providing calibrated EUV spectral measurements for over four years.

This paper is divided into seven sections. The TIMED spacecraft operations are described first, then the orbit change determination method is presented, followed by the orbit change validation section, a brief introduction to the SEE instrument, one-band correlations of solar irradiance in broad and narrow bands with the orbit change, two-band correlations, and conclusions.

A power-law relationship is observed between the daily-averaged negative time derivative of the TIMED semimajor axis D and daily-averaged broadband solar EUV irradiance measurements. A correlation of about 93% is found between SEE measurements integrated from 27–105 nm and D. A similar comparison using the 10.7-cm solar radio flux ($F_{10.7}$) proxy is also presented, which shows a significantly lower correlation. This work demonstrates the need for continued EUV monitoring for satellite-drag studies and provides a simple method for estimating drag operationally. Furthermore, as solar EUV predictive quality increases with forecasting models, this straightforward approach will allow more accurate prediction of satellite drag.

II. TIMED Spacecraft, Orbit, and Operations

The TIMED spacecraft was launched on 7 December 2001 into an approximately circular orbit with a 74.1-deg inclination and an altitude of about 625 km. Since then, the orbit has decayed slightly due to the friction of impinging atoms and molecules. During normal operations, TIMED is three-axis stabilized and nadir-pointing, with the x axis aligned with the ram direction. The orbit was chosen as a convenience for the other instruments on TIMED and allows nearly the same coverage of the Earth from one calendar year to the next. The shape of the TIMED spacecraft body can be adequately approximated by a cuboid with rectangular x and y faces and square z faces. Two instruments and the star trackers are attached to the $-z$ (negative z direction) deck with a modest extension, and the other

Presented as Paper 6169 at the AIAA/AAS Astrodynamics Specialist Conference and Exhibit, Keystone, CO, 21–24 August 2006; received 31 October 2006; revision received 11 March 2007; accepted for publication 10 May 2007.

*Professional Research Assistant, Laboratory for Atmospheric and Space Physics, Mission Operations and Data Systems Division, Campus Box 590. Member AIAA.

†Associate Director, Laboratory for Atmospheric and Space Physics, Technical Division, Campus Box 590. Member AIAA.

‡Research Scientist, Laboratory for Atmospheric and Space Physics, Science Division, Campus Box 590. Member AIAA.

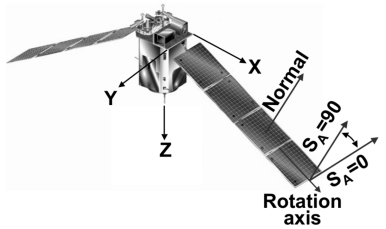

Fig. 1 Artist's concept of the TIMED spacecraft, shown with the panels oriented in the 90-deg position of the solar panel rotation angle S_A. (Courtesy of NASA and Johns Hopkins University Applied Physics Laboratory.)

two instruments are recessed. The instrument extensions are largely constant with time, and there would be little area change along the x axis if not for the solar panels, as shown in Fig. 1. The panels are significantly longer than the spacecraft body and extend out from both x faces of the spacecraft at an angle of 20 deg from the normal of each face. The solar panel centerline is the rotation axis for the panel and maintains this fixed 20-deg angle. The solar panel rotation angle (S_A, shown in Fig. 1) defines the rotation of the panel about the centerline. Note that x is along the direction of travel. The panels rotate to minimize the angle defined by the panel normal to the sun vector at the location in the orbit where the spacecraft is closest to the sun. The rotation of the solar panels can range from 0 to 90 deg, and 90 deg is shown in Fig. 1. In a typical day, the panels rotate by about 3 deg.

In this study, we assume that the angle of solar panel rotation leads only to increased total surface area facing the direction of travel, as shown in Fig. 2. This implies that the speed of TIMED ($\sim$7.5 km/s) is much larger than the speed of particles in the atmosphere with which it is colliding. The area correction factor is a maximum when S_A is 90 deg and a minimum when S_A is 0 deg. The area correction factor is used to suppress the effect of changes in the spacecraft-shape facing ram, which induce changes in the actual drag. Because these changes that result from the spacecraft solar panel rotation angle do not represent atmospheric density changes, they are removed. With this correction applied, the drag rate better represents the atmospheric density changes and is no longer dependent upon the geometry of the spacecraft. A correction factor value of 1.0 corresponds to the normal to the panels being oriented perpendicular to the ram ($-Y$) direction, and so the solar panels do not contribute any appreciable area. TIMED provides an excellent platform for studying the effects of atmospheric drag on the satellite, because the spacecraft form factor facing the velocity direction changes only by the orientation of the solar arrays. TIMED has no propulsion system, and so there are no station-keeping maneuvers to consider.

The angle S_A is not available in any standard data product. The orientation angle was extracted from the unprocessed spacecraft telemetry packets and converted into units of degrees. Data were retrieved over the entire mission then averaged to create a daily mean.

The largest area change is less than 8% and occurs near the periodic yaw maneuvers. The angle S_A usually does not drop below 30 deg. Those periods correspond to times when the spacecraft is sunlit for nearly the entire orbit and there is plenty of power available,

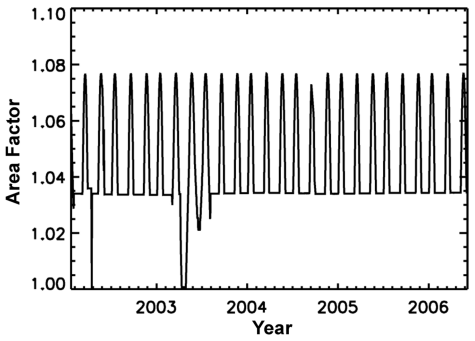

Fig. 2 Multiplicative area correction factor.

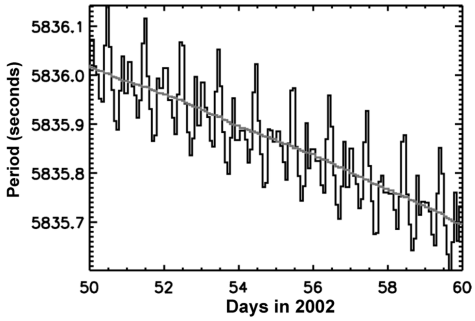

Fig. 3 Nodal period (in seconds) for each orbit (jagged line) over 10 days in 2002; the diagonal curve is geopotential-corrected (see Fig. 4).

and so fine-tuning the solar panel orientation is not necessary. One X face of the spacecraft (say, $+X$) faces toward the velocity vector for about 63 days, after which the spacecraft orbit has precessed and the spacecraft maneuvers to point the opposite face ($-X$) toward the velocity vector. This is a yaw maneuver (rotation about the Z axis) and can be completed within about 30 min. SEE must remain on the sunlit side to support normal operations, and the routine spacecraft maneuvers ensure that this occurs.

The global position system (GPS) navigation system [4] onboard TIMED provides a three-sigma position accuracy to 300 m every second and three-sigma velocity accuracy to 25 cm/s. This translates into an absolute position knowledge uncertainty of about 4.0% of the distance traveled between each 1-Hz sample. Performance assessments performed in-flight indicate that positional accuracy agrees with radar-tracking estimates within a maximum difference of 50 m (0.67%), depending on the specific verification method [4]. This is sufficient accuracy for this study.

The position of TIMED is recorded in a standard product at the TIMED mission data center.[§]

III. TIMED Orbit Change Determination Method

In this section, we focus on estimating the daily-averaged nodal period to determine the orbit changes for TIMED. The position is reported by the onboard GPS navigation system in an Earth-centered inertial reference frame at 1 Hz [4]. The nodal periods are determined by interpolation of the time of 1-s GPS position samples to the ascending node (northward equatorial crossings). About 14.8 nodal-period measurements are available for TIMED in each Universal Time (UT) day, and the daily variation in the nodal period is shown by the jagged line in Fig. 3. The diagonal curve in Fig. 3 is determined from correcting the geopotential effect shown in Fig. 4. The effective semimajor axis a is then calculated using Kepler's law of periods. Although the orbit is non-Keplerian and this assumption breaks down for period estimations using intervals smaller than an orbit [5], it works fairly well for integer numbers of orbits. However, there is a small perturbing gravitational effect of Earth's nonuniform mass distribution that makes this analysis more difficult [6]. A geographical longitude dependence of the period for each orbit is observed (see Fig. 4) and was largely suppressed (diagonal line in Fig. 3) through application of a correction and a fitted residual. This correction to the nodal period is most likely due to nonuniformities in the gravitational field near the equator. Because the nodal periods are derived from timing measurements of ascending equator crossings, these nonuniformities appear to be the cause of local accelerations we observe near the equator. The Earth's gravitational field variation is noticeable when the nodal periods are plotted as a function of ascending node longitude, as in Fig. 4. The shape is very repeatable over 20,000 orbits, with a spread of a few tens of milliseconds in each 1-deg bin. Direct comparison to other measurements of the geopotential [7] was not performed and remains the subject of future work. After the correction including the residual, there remains a

[§]Files containing the actual position, velocity, attitude, and time are available online in network common data form (netCDF) format at http://www.timed.jhuapl.edu/WWW/mdc/data/OrbitFiles/ [retrieved 2 July 2007].

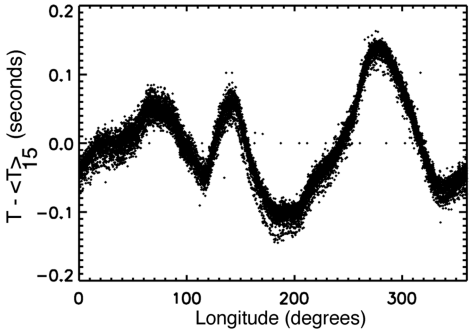

Fig. 4 Nodal periods differenced with the running 15-orbit vs geographic longitude; over 20,000 orbits are shown.

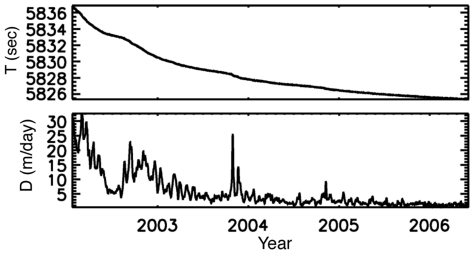

Fig. 5 Corrected nodal period (in seconds) for the TIMED mission and the drag rate *D*.

one-sigma spread of periods over all 360 bins of less than 4 ms that is not removed. The nodal period that is obtained from this method provides sufficient accuracy for this study, because we then average the corrected nodal periods over each UT day.

Figure 5 shows the daily-averaged nodal period for the TIMED mission. Any of the remaining short-term effects are smaller than the daily nodal-period changes. With the daily-averaged nodal period, we can then apply Kepler's law to determine the semimajor axis a for an equivalent Keplerian orbit and avoid problems with osculating elements [5]. We find it convenient to define a term to represent the drag rate as a scalar speed to quantify the decrease of a with time. The drag rate D is thus defined as the negative time derivative of a. Because the decreases are small for TIMED, we choose to represent D in units of meters per day. This is shown in Fig. 5 and shows similar variability to the measured solar EUV irradiance [2], as shown in Sec. VII. Strong solar rotations are noticeable in 2002 through 2003 and particularly around the well-known "Halloween" flares of 2003 [8].

IV. Orbit Change Validation

The validation of the orbit determination method described earlier is presented in this section. For validation, we use the historical two-line element (TLE) sets provided by the U.S. Department of Defense.[¶] We choose to examine the first time derivative of the mean motion for comparison, $\mathrm{d}n/\mathrm{d}t$. For qualitative comparison, we will compare the daily-averaged D described in the previous section with $\mathrm{d}n/\mathrm{d}t$ (see Fig. 6).

We calculate a daily average value of $\mathrm{d}n/\mathrm{d}t$ because some days have multiple TLEs available. Although $\mathrm{d}n/\mathrm{d}t$ is only used in simplified general perturbation (SGP), it is quite adequate for qualitative comparisons, because the TIMED orbit is nearly circular and in low-Earth orbit. This orbit was shown in the previous section to be dominated by Earth gravity and atmospheric drag, in accordance with the SGP model assumption.

Figure 5 shows the drag rate D as determined from GPS nodal period averaging. In Fig. 7, $\mathrm{d}n/\mathrm{d}t$ is taken from the TLE term. The plot shows $\mathrm{d}n/\mathrm{d}t$, which was simply scaled by the ratio of the means. Although the two quantities have a linear correlation of 0.956 over the mission, this is lowered by the fact that the TLE solutions do not have accompanying integration times. It is not possible to determine if the solution was generated using information from 1–30 days of tracking, and so the center time can only be estimated. During late 2005, a time range of 13 days was used for determining the solutions. We determined the best offset for the TLE center time using six-month periods. In Fig. 6, the drag rate is shown with the shifted TLE $\mathrm{d}n/\mathrm{d}t$. This demonstrates the crossover from a four-day lag to a two-day lag. The lag time was calculated by minimizing the squared difference of the two curves by varying one relative to the other in integral day numbers. The two curves show excellent agreement up through the end of 2004. After that period, the TLEs become significantly more noisy as the decay rates become very small. The result of looking at the whole mission is that there is a variable day-shift ranging from 2–5 days in the TLE data, which will complicate comparisons to historical TLE sets. This indicates that the duration of tracking data used to create the TLEs may have changed over the mission. High correlations of over 0.97 can be achieved in individual six-month intervals by minimizing the sum of the squared differences. A similar analysis was performed using the B^* drag term with nearly identical results. In summary, the drag rate determination method using GPS positioning and timing measurements was validated with the best available independent TLE information. The onboard GPS navigation system on TIMED provides estimates of the satellite drag that are sensitive enough to allow detection of small changes in the way TLEs were calculated.

V. SEE Instrument

At present, SEE is the only instrument measuring the full solar EUV irradiance from 27–115 nm [2,9]. The SEE instrument is composed of two scientific components to measure the full-disk solar irradiance from 0.1–193 nm. One component is the x-ray ultraviolet (XUV) photometer system (XPS), which contains an array of broadband photometers for wavelengths less than 27 nm [10]. The other component is an EUV grating spectrograph (EGS), which provides spectra of the solar EUV and FUV at 0.4-nm resolution from 27–193 nm [11,12].

SEE has been described elsewhere in detail [2,9] and provides the best absolute calibrated solar EUV measurements to date [10–14].

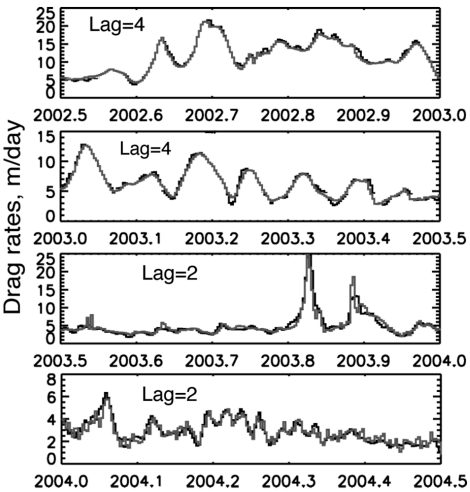

Fig. 6 *D* and $\mathrm{d}n/\mathrm{d}t$ (gray) with a varying lag.

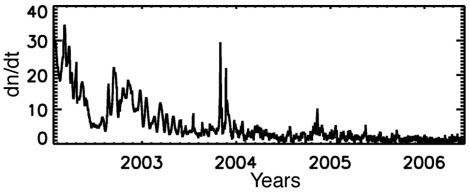

Fig. 7 First time derivative of the mean motion ($\mathrm{d}n/\mathrm{d}t$) from TLEs.

[¶]Data available online at http://www.space-track.org/perl/login.pl [retrieved 9 June 2006].

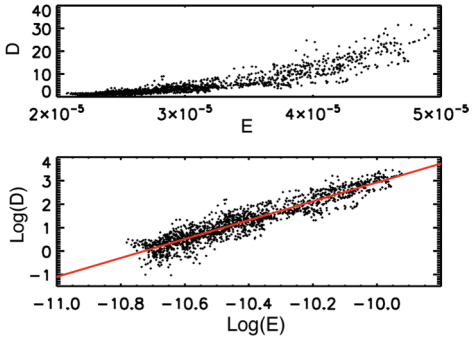

Fig. 8 D (m/day) vs E (integrated solar EUV from 27–105 nm W/m^2); the lower graph shows a best-fit line, with a slope of 4.02 ± 0.04 indicating a power law.

The initial calibration for the EGS was performed at the National Institutes for Standards and Technology (NIST) Synchrotron Ultraviolet Radiation Facility (SURF). Absolute calibration accuracy is maintained through periodic suborbital rocket underflights with similar instruments that are also calibrated at the NIST-SURF [14].

All SEE data used in this paper are from release version 8.** Version 8 data products are routinely generated after two days, but are reprocessed after 30 days to provide higher-quality solar irradiances. A special low-latency space weather product is also available with a subset of the latest available measurements. SEE measurements are providing the standard for EUV irradiance measurements and have been incorporated into the popular SOLAR2000 model [3] since 2004.

VI. One-Band Correlation Study

In this section, we report results from the study of the relationship of solar EUV measured by SEE to the atmospheric drag experienced by TIMED. The dominant species in the altitude range of TIMED is atomic oxygen, which has a cross section that is large in the EUV and decreases for wavelengths exceeding 105 nm. We therefore studied the integrated EUV E from 27–105 nm.

A first attempt at determining a relationship began by observing a curved shape in a plot of the daily-averaged E and the daily-averaged D. This is shown in Fig. 8 as a power-law relationship with an exponent of approximately 4.02. Very small changes in the EUV have tremendous effects on the spacecraft drag force. The correlation between the base-10 logarithm of E and the base-10 logarithm of D exceeds 0.930. Although we do not expect perfect correlation, this result is very promising.

We then performed a similar analysis using $F_{10.7}$, which is often used as a proxy for the EUV and which gave a correlation of about 0.898. Although $F_{10.7}$ was used to provide a long-term record of solar activity, it is found to be inferior to direct measurement of the solar EUV by TIMED-SEE.

It should be noted that other wavelength bands were also studied. A selection of these is presented in Table 1. For small changes in wavelength range, the correlations only change by a small amount. For example, the 27–115-nm band yields essentially no difference from 27–105 nm. Extending the lower limit down to 0.1 nm, however, does increase the correlation slightly, up to 0.934. Because the gain is marginal, alternate bands may be preferred. Future missions with different instrument-specific bands may produce similar results, provided that the absolute calibration is comparable to TIMED-SEE. Until the soft x-ray portion of the solar spectrum is measured at high resolution for at least half of a solar cycle, the correlations will remain limited to broadband.

**SEE measurements are available in netCDF format, along with software for reading the data in interactive data language (IDL), at http://lasp.colorado.edu/see [retrieved 2 July 2007].

Table 1 One-term correlation results

One-term correlations of D vs E		
E	Correlation	Exponent
27–105 nm	0.929	4.02
121–122 nm	0.914	6.79
0.1–105 nm	0.934	3.86
0.1–115 nm	0.935	3.97
27–34 nm	0.928	3.52
$F_{10.7}$	0.897	2.70

VII. Two-Band Correlation Study

One EUV band was chosen for the one-band correlation study, because the direct heating of the thermosphere occurs through the excess energy released from ionization. The previous section uses data from one instrument to achieve a relatively high degree of correlation, but should not be expected to capture the complete behavior. One method to improve upon the basic principle involves using other distinct bands to allow for different physical processes to contribute in differing amounts. This is the same basic machinery used in traditional proxy modeling. However, instead of using proxies, in this case we use measurements of the FUV. FUV photons are absorbed by O_2 molecules in the Schuman–Runge continuum and contribute to thermospheric heating. The excess energy then propagates upward with some delay. This is a complicated process because it depends upon many factors, and so the delay time may range from hours to days, depending on the altitude in which the energy is deposited. The delay time is expected to depend on the altitude in which the energy is absorbed, the temperature of the absorbers, and the efficiency of vertical transport. These effects may contribute to smoothing out the delay time. This two-band correlation study allows EUV to provide direct heating and allows FUV to provide a delayed heating.

We represent the two-band irradiance function as $E_{2\text{-band}}$ and compare it against D. We examined numerous FUV bands using linear regression to maximize the correlation with D. Some of the bands we considered are summarized in Table 2. The EUV band described in the previous section was used as one term, and the FUV portion was varied to arrive at a maximum correlation of over 0.949 using the 147–165-nm band. This band was found by allowing the FUV short- and long-wavelength bins to change independently. The FUV bands were also allowed to lag by an integer number of days. The lag of one day provides the maximum correlation, but two- and three-day lags are very similar. The best combination found involves the 0.1–105-nm EUV band with no lag, and the 147–165-nm FUV band with a one-day lag, which we define as $E_{2\text{-band}}$.

The top panel of Fig. 9 shows $F_{10.7}$ scaled to match the units of D. There is significant disagreement in 2002. In general, $F_{10.7}$ tends to have larger solar rotational variability than D. The lower panel of Fig. 9 shows D and $E_{2\text{-band}}$, which has also been scaled to the units of D. The two-band irradiance function is significantly better at approximating D.

The differences between the two-band irradiance function and D can be attributed to many sources. Perhaps the most significant source of disagreement is caused by the 3% duty cycle of SEE. The

Table 2 Two-term correlation results

One-term correlations of D vs E			
EUV	FUV	FUV lag, days	Correlation
27–105	121–122	0	0.932
27–105	147–165	0	0.945
27–105	147–165	0	0.945
27–105	147–165	0	0.945
27–105	147–165	1	0.946
27–105	147–165	2	0.944
27–105	147–165	3	0.938
0.1–105	147–165	1	0.949

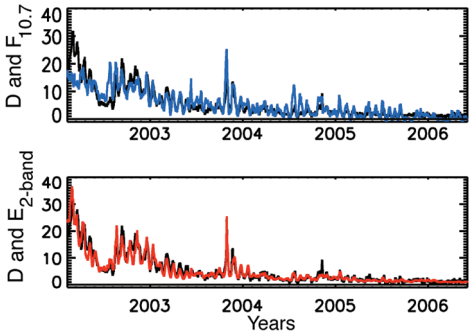

Fig. 9 ***D*** **(black) with scaled** $F_{10.7}$ **(blue) and** $E_{2\text{-band}}$ **(red).**

atmosphere responds to all Earth-directed radiation; however, SEE is only sampling the daily irradiance. Many large flares are completely missed by SEE. The quality of the FUV measurement for TIMED-SEE is low compared with other measurements such as SORCE-SOLSTICE [15–17], although the FUV variability is small. However, those measurements did not begin until early 2003, and the spectrometer scanning routine of SOLSTICE prevents simultaneous measurement of the entire FUV-wavelength range. Atmospheric preconditioning may also play a role that could cause disagreement. Nevertheless, the one- and two-band irradiance functions may provide an improvement over previous drag models [18–20], some of which have 15% standard deviation, and may be useful operationally.

VIII. Conclusions

SEE is providing high-quality, calibrated, daily solar EUV irradiance measurements that show remarkably good agreement with the daily TIMED spacecraft drag. A strong power-law relationship is observed between the time derivative of the TIMED semimajor axis and the SEE EUV irradiance measurements. A correlation of about 93% is found, indicating that it may be possible to predict the satellite semimajor axis change with accurate EUV measurements and may be useful for satellite operations. A similar comparison using $F_{10.7}$ shows a significantly lower correlation. A more sophisticated two-band correlation method was shown to produce correlations of nearly 95%. This work demonstrates the need for continued EUV monitoring for satellite-drag studies. SEE was approved for continued operations through 2010. Future missions will provide real-time continuous solar EUV monitoring capabilities on National Oceanic and Atmospheric Administration (NOAA) geostationary operational environmental satellites and the NASA Solar Dynamics Observatory (SDO). SDO is scheduled for launch in August 2008.

Although a high correlation exists, it is unrealistic to expect better correlations using only solar irradiance measurements. Although solar irradiance is the dominant mechanism for thermospheric heating, solar energetic particles and geomagnetic activity effects also contribute to the heating. It may be fortuitous that during periods when many energetic particles are flowing into the atmosphere, the solar EUV is also elevated. Also, the TIMED orbit does not travel above 74.1 deg in latitude (where much of the particle energy is deposited), and so the effect may be further suppressed for this spacecraft. Geomagnetic heating of the thermosphere has been discussed by others [21], but it is not expected to have a significant affect on the altitude region of this study [22].

At present, there is no comprehensive theoretical treatment of the effect of solar EUV on thermospheric neutral density changes, due in part to the rich chemistry and coupled nature of the upper-atmosphere dynamics and energy-exchange mechanisms. This study circumvents these problems and also diurnal differences by converting the daily-averaged TIMED spacecraft orbit changes into a direct measure of relative neutral density changes, which we choose to express as a time rate of change of the semimajor axis. Problems associated with time-of-day passage through the diurnal bulge are smoothed away by daily averaging, and all of the complications of energy absorption and transfer and cross sections are encapsulated in the power-law result. Application of the results discussed in this paper to noncircular orbiting spacecraft are nontrivial and require more detailed knowledge of the spacecraft orientation and geometry, periapsis timing, and higher time-cadence measurements of solar EUV variation.

If accurate predictive solar EUV forecasting models were available, this simple power-law approach would allow accurate predictions of thermospheric density near 600 km and, hence, satellite drag. This method may be extended to other spacecraft for daily average comparisons.

Acknowledgments

D. L. Woodraska would like to thank M. Packard at the Johns Hopkins University Applied Physics Laboratory (JHU/APL) for discussions about the Thermosphere–Ionosphere–Mesosphere Energetics and Dynamics (TIMED) spacecraft and assistance provided, and B. Bowman at Peterson Air Force Base for enlightening discussions. This work would not have been possible without the numerous operators, engineers, staff, and scientists at the Laboratory for Atmospheric and Space Physics and JHU/APL who have contributed to the success of the Solar Extreme-Ultraviolet Experiment instrument and the TIMED mission.

References

[1] Chamberlain, J. W., *Theory of Planetary Atmospheres: An Introduction to Their Physics and Chemistry*, Academic Press, New York, 1978.

[2] Woods, T. N., Eparvier, F. G., Bailey, S. M., Chamberlin, P. C., Lean, J., Rottman, G. J., Solomon, S. C., Tobiska, W. K., and Woodraska, D. L., "Solar EUV Experiment (SEE): Mission Overview and First Results," *Journal of Geophysical Research, Space Physics*, Vol. 110, No. A1, Jan. 2005, Paper A01312.

[3] Tobiska, W. K., Woods, T., Eparvier, F., Viereck, R., Floyd, L., Bouwer, D., Rottman, G., and White, O. R., "The SOLAR2000 Empirical Solar Irradiance Model and Forecast Tool," *Journal of Atmospheric and Solar-Terrestrial Physics*, Vol. 62, Sept. 2000, pp. 1233–1250.

[4] Devereux, W. S., Asher, M. S., Heins, R. J., Chacos, A. A., Kusterer, T. L., and Linstrom, L. A., "TIMED GPS Navigation System (GNS): Design, Implementation, and Performance Assessment," *Johns Hopkins APL Technical Digest*, Vol. 24, 2003, pp. 179–193.

[5] Goldstein, H., *Classical Mechanics*, 2nd ed., Addison Wesley Longman, Reading, Mass, 1980.

[6] Picone, J. M., Emmert, J. T., and Lean, J. L., "Thermospheric Densities Derived from Spacecraft Orbits: Accurate Processing of Two-Line Element Sets," *Journal of Geophysical Research, Space Physics*, Vol. 110, Mar. 2005.

[7] Tapley, B., Ries, J., Bettadpur, S., Chambers, D., Cheng, M., Condi, F., Gunter, B., Kang, Z., Nagel, P., Pastor, R., Pekker, T., Poole, S., and Wang, F., "GGM02—An Improved Earth Gravity Field Model from GRACE," *Journal of Geodesy*, Vol. 79, Nov. 2005, pp. 467–478.

[8] Woods, T. N., Eparvier, F. G., Fontenla, J., Harder, J., Kopp, G., McClintock, W. E., Rottman, G., Smiley, B., and Snow, M., "Solar Irradiance Variability During the October 2003 Solar Storm Period," *Geophysical Research Letters*, Vol. 31, No. 10, May 2004, Paper L10802.

[9] Woods, T. N., Bailey, S., Eparvier, F., Lawrence, G., Lean, J., McClintock, B., Roble, R., Rottman, G. J., Solomon, S. C., Tobiska, W. K., and White, O. R., "TIMED Solar EUV Experiment," *Physics and Chemistry of the Earth, Part C: Solar-Terrestial and Planetary Science*, Vol. 25, Nos. 5–6, 2000, pp. 393–396.

[10] Woods, T. N., Rottman, G., and Vest, R., "XUV Photometer System (XPS): Overview and Calibrations," *Solar Physics*, Vol. 230, Aug. 2005, pp. 345–374.

[11] Eparvier, F. G., Woods, T. N., Ucker, G., and Woodraska, D. L., "TIMED Solar EUV Experiment: Pre-Flight Calibration Results for the EUV Grating Spectrograph," *Proceedings of the SPIE*, Vol. 4498, International Society For Optical Engineering , Bellingham, WA, 2001, p. 91.

[12] Woodraska, D. L., Woods, T. N., and Eparvier, F. G., "In-flight Calibration and Performance of the Solar Extreme Ultraviolet Experiment (SEE) Aboard the TIMED Satellite," *Proceedings of the SPIE*, Vol. 5660, International Society for Optical Engineering , Bellingham, WA, 2004, pp. 36–47.

[13] Woods, T. N., and Eparvier, F. G., "Solar Ultraviolet Variability During the TIMED Mission," *Advances in Space Research*, Vol. 37, No. 2, 2006, pp. 219–224.

[14] Woods, T. N., Rottman, G. J., and Solomon, S. C., "Solar Extreme Ultraviolet Irradiance Measurements from Sounding Rockets During Solar Cycle 22," *Physics and Chemistry of the Earth, Part C: Solar-Terrestial and Planetary Science*, Vol. 25, Nos. 5–6, 2000, pp. 397–399.

[15] McClintock, W. E., Rottman, G. J., and Woods, T. N., "Solar-Stellar Irradiance Comparison Experiment 2 (SOLSTICE 2): Instrument Concept and Design," *Solar Physics*, Vol. 230, Aug. 2005, pp. 225–258.

[16] McClintock, W. E., Snow, M., and Woods, T. N., "Solar-Stellar Irradiance Comparison Experiment 2 (SOLSTICE 2): Pre-Launch and On-Orbit Calibrations," *Solar Physics*, Vol. 230, Aug. 2005, pp. 259–294.

[17] Snow, M., McClintock, W. E., Rottman, G., and Woods, T. N., "Solar-Stellar Irradiance Comparison Experiment 2 (SOLSTICE 2): Examination of the Solar-Stellar Comparison Technique," *Solar Physics*, Vol. 230, Aug. 2005, pp. 295–324.

[18] Storz, M. F., Bowman, B. R., Branson, M. J. I., Casali, S. J., and Tobiska, W. K., "High Accuracy Satellite Drag Model (HASDM)," *Advances in Space Research*, Vol. 36, No. 12, 2005, pp. 2497–2505.

[19] Marcos, F. A., "New Satellite Drag Modeling Capabilities," *44th AIAA Aerospace Sciences Meeting and Exhibit*, AIAA, Reston, VA, 2006, pp. 1–13; also AIAA Paper 2006-470.

[20] Doornbos, E., Klinkrad, H., and Visser, P., "Atmospheric Density Calibration Using Satellite Drag Observations," *Advances in Space Research*, Vol. 36, No. 3, 2005, pp. 515–521.

[21] Knipp, D. J., Tobiska, W. K., and Emery, B. A., "Direct and Indirect Thermospheric Heating Sources for Solar Cycles 21–23, *Solar Physics*, Vol. 224, Oct. 2004, pp. 495–505.

[22] Bowman, B. R., and Storz, M. F., "High Accuracy Satellite Drag Model (HASDM) Review," *Astrodynamics 2003*, Advances in the Astronautical Sciences, Vol. 116, Part 3, Univelt, San Diego, CA, 2003, p. 1943.

A. Ketsdever
Associate Editor